

# Cubic-Quintic Long-Range Interactions With Double Well Potentials

P.A. Tsilifis

*Department of Mathematics, University of Southern California, Los Angeles, 90089-2532 CA, USA*

P.G. Kevrekidis

*Department of Mathematics and Statistics, University of Massachusetts, Amherst, MA 01003-9305, USA*

V.M. Rothos

*Department of Mathematics, Physics Computational Sciences, Faculty of Engineering,  
Aristotle University of Thessaloniki, Thessaloniki 54124, Greece*

In the present work, we examine the combined effects of cubic and quintic terms of the long range type in the dynamics of a double well potential. Employing a two-mode approximation, we systematically develop two cubic-quintic ordinary differential equations and assess the contributions of the long-range interactions in each of the relevant prefactors, gauging how to simplify the ensuing dynamical system. Finally, we obtain a reduced canonical description for the conjugate variables of relative population imbalance and relative phase between the two wells and proceed to a dynamical systems analysis of the resulting pair of ordinary differential equations. While in the case of cubic and quintic interactions of the same kind (e.g. both attractive or both repulsive), only a symmetry breaking bifurcation can be identified, a remarkable effect that emerges e.g. in the setting of repulsive cubic but attractive quintic interactions is a “symmetry restoring” bifurcation. Namely, in addition to the supercritical pitchfork that leads to a spontaneous symmetry breaking of the anti-symmetric state, there is a subcritical pitchfork that eventually reunites the asymmetric daughter branch with the anti-symmetric parent one. The relevant bifurcations, the stability of the branches and their dynamical implications are examined both in the reduced (ODE) and in the full (PDE) setting.

## I. INTRODUCTION

In the study of both atomic and optical physics problems, often analyzed in the realm of nonlinear Schrödinger type equations [1, 2], the study of double well potentials has a prominent position. Such potentials can be straightforwardly realized in atomic Bose-Einstein condensates (BECs) through the combination of a parabolic (harmonic) trap with a periodic potential. Their experimental realization and subsequent study in BECs with self-repulsive nonlinearity has led to numerous interesting observations including tunneling and Josephson oscillations for small numbers of atoms in the condensate, and macroscopic quantum self-trapped states for large atom number [3] and symmetry-breaking dynamical instabilities [4]. These experimental developments have been accompanied by a larger array of theoretical studies on issues such as finite-mode reductions and symmetry-breaking bifurcations [5–12], quantum effects [13], and nonlinear variants of the potentials [14]. Similar features have also emerged in nonlinear optical settings including the formation of asymmetric states in dual-core fibers [15], self-guided laser beams in Kerr media [16], and optically-induced dual-core waveguiding structures in photorefractive crystals [17].

On the other hand, a theme that has also been progressively becoming of increasing importance within both of these areas of physics is that of long range interactions. In the atomic context, the experimental realization of BECs of magnetically polarized  $^{52}\text{Cr}$  atoms [18] (see recent review [19] and for a study of double well effects [20]), as well as the study of dipolar molecules [21], and atoms in which electric moments are induced by a strong external field [22] have been at the center of the effort to appreciate the role of long range effects. On the other hand, in nonlinear optics, where nonlocal effects have been argued to be relevant for some time now [23], numerous striking predictions and observations have arisen in the setting of thermal nonlocal media. Among them, we single out the existence of stable vortex rings [24] the experimental realization of elliptically shaped spatial solitons [25] and the observation of potentially pairwise attracting (instead of repelling as in the standard local cubic media) dark solitons [26].

Our aim in the present work is to expand on the framework of studies of double well potentials in the presence of nonlocal nonlinear interactions by considering cubic-quintic models. Part of the motivation for doing so consists of the fundamental relevance of the cubic-quintic nonlinear Schrödinger. The latter is a model that has been used in a variety of physical settings. These include the light propagation in optical media such as non-Kerr crystals [27], chalcogenide glasses [28], organic materials [29], colloids [30], dye solutions [31], and ferroelectrics [32]. It has also been predicted that this type of nonlinearity may be synthesized by means of a cascading mechanism [33]. An additional part of the motivation stems from an interesting set of observations that were made in an earlier work featuring competing *cubic* nonlinearities, one of which was a cubic local and another was a cubic nonlocal one; see [34] and the discussion therein. In that work, it was found that for repulsive nonlocal cubic interactions and attractive local ones, it was

possible to tune the prefactors determining the competition so as to produce not only a symmetry breaking, but also a symmetry-restoring bifurcation. More recently, a similar conclusion in a local cubic-quintic double well potential was reached in [35].

Here, we present a framework where the competition of cubic and quintic terms can be systematically quantified. In addition, to address the problem from a broader perspective, we consider fully nonlocal interactions both for the cubic and the quintic terms, rendering the local case a straightforward special-case scenario of our study. We start our presentation of the theoretical analysis of section II by developing a two-mode reduction of the system with both the cubic and the quintic terms. We systematically examine all the relevant terms and offer a prescription for assessing the dominant contributions to the resulting dynamics of the left and the right well. Following an amplitude-phase decomposition and examining the variables associated with the population imbalance of the two wells, and their relative phase, we construct the Hamiltonian normal form of the two-mode reduction of the cubic-quintic double well system. We then *explicitly illustrate* how the bifurcation analysis of this normal form encapsulates not only the symmetry breaking but *also* the symmetry restoring. We argue that this cubic-quintic realization is the prototypical one where both of these effects can be observed and analytically quantified. Subsequently, in section III, we proceed to test the relevant predictions by means of a computational bifurcation analysis, as well as through direct numerical simulations (in order to monitor the predicted dynamical instabilities). We find very good agreement with the symmetry breaking predictions of the model and even a quite fair agreement with the symmetry restoring ones (which arise in a highly nonlinear regime and are hence less amenable to a two-mode analysis). We also quantify the disparity of the analytical predictions and numerical results for large values of the nonlocality range parameter. Finally, section IV contains our conclusions and some directions for future study.

## II. ANALYTICAL APPROACH FOR THE NLS EQUATION WITH TWO NONLOCAL TERMS

### A. Two-mode approximation

As indicated above, our fundamental model will be the 1d NLS equation in the presence of two nonlocal terms, namely the cubic and quintic ones:

$$i\partial_t\psi + \mu\psi = \mathcal{L}\psi + s \left( \int_{-\infty}^{+\infty} R_1(x-x')|\psi(x')|^2 dx' \right) \psi + \delta \left( \int_{-\infty}^{+\infty} R_2(x-x')|\psi(x')|^4 dx' \right) \psi \quad (1)$$

with  $s, \delta = \pm 1$  and the linear operator will be of the standard Schrödinger type

$$\mathcal{L} = -(1/2)\partial_x^2 + V(x).$$

This encompasses the double-well potential of the form:

$$V(x) = (1/2)\hat{\Omega}^2 x^2 + V_0 \text{sech}^2(x/w)$$

with  $\hat{\Omega}$  being the normalized strength of the parabolic trap and it is  $\hat{\Omega} \ll 1$  in a quasi-1d situation in BECs (here the effective trap frequency is the ratio of the longitudinal trap strength along the condensate over the one of the tightly confined transverse directions). In our study we consider a typical experimentally relevant value of  $\hat{\Omega} = 0.1$ , while the generally tunable (see e.g. [36]) parameters of the laser beam forming the light defect are chosen to be  $V_0 = 1$  and  $w = 0.5$  (which we have found to be fairly typical values representative of the phenomenology to be analyzed below).

For the kernels  $R_1, R_2$  we will focus our considerations on either the Gaussian

$$R_i(x) = \frac{1}{\sigma\sqrt{\pi}} \exp(-\frac{x^2}{\sigma^2})$$

or the exponential

$$R_i(x) = \frac{1}{2\sigma} \exp(-\frac{|x|}{\sigma}),$$

in the spirit of the works of [23]. The key parameter here is the range of the nonlocal interaction parametrized by  $\sigma$ . Notice that both kernels in the limit of  $\sigma \rightarrow 0$  tend to a genuinely local interaction (i.e.,  $R_i(x) \rightarrow \delta(x)$ ).

We now develop the two-mode approximation in order to obtain a decomposition (or more accurately a Galerkin truncation) of the solution  $\psi$  over the minimal basis of fundamental states. More specifically, we use an orthonormal basis composed by the wave functions  $\{\phi_L, \phi_R\} \equiv \{(u_0 - u_1)/\sqrt{2}, (u_0 + u_1)/\sqrt{2}\}$ , where  $u_0$  and  $u_1$  (Fig. 1) are

the ground state and the first excited state, respectively, corresponding to the first two eigenvalues of  $\mathcal{L}$  that are  $\omega_0 = 0.13282$  and  $\omega_1 = 0.15571$  for our choice of potential parameters above. Notice that these two eigenfunctions represent modes with support predominantly on the left and right well, respectively. The eigenfunctions  $u_{0,1}$  and the rotated basis employed herein of  $\phi_{L,R}$  are both shown in Fig. 1.

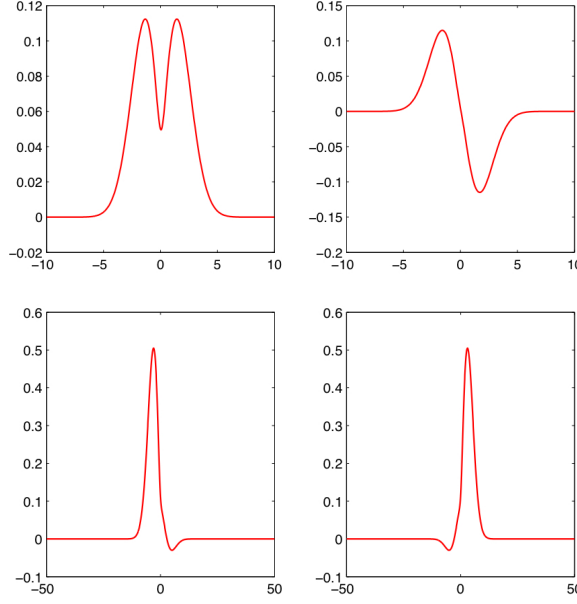


FIG. 1: The ground state  $u_0$  and first excited state  $u_1$  of the potential are shown in the top panel. The rotated orthonormal basis of  $\phi_L$  and  $\phi_R$  (with support, respectively, on the left and right well) is shown in the bottom panels.

The two-mode approximation is then defined as

$$\psi(x, t) = c_L(t)\phi_L(x) + c_R(t)\phi_R(x) \quad (2)$$

where  $c_L$  and  $c_R$  are complex time-dependent amplitudes and the approximation consists of the truncation of the higher modes within the expansion. Before substituting into the initial GP equation, we notice that the action of the linear operator  $\mathcal{L}$  on our basis elements is as follows:

$$\mathcal{L}\psi = (\Omega c_L - \omega c_R)\phi_L + (\Omega c_R - \omega c_L)\phi_R$$

where  $\Omega = (\omega_0 + \omega_1)/2$  and  $\omega = (\omega_1 - \omega_0)/2$  are linear combinations of the two eigenvalues of  $\mathcal{L}$  respectively to the solutions  $u_0, u_1$ . Subsequently, substitution of our ansatz of Eq. (2) in the full nonlinear problem of Eq. (1) yields:

$$\begin{aligned} i\dot{c}_L\phi_L + i\dot{c}_R\phi_R = & (\Omega c_L - \mu c_L - \omega c_R)\phi_L + (\Omega c_R - \mu c_R - \omega c_L)\phi_R + \\ & + s|c_L|^2(c_L\phi_L + c_R\phi_R) \int R_1(x-x')\phi_L^2(x')dx' + s|c_R|^2(c_L\phi_L + c_R\phi_R) \int R_2(x-x')\phi_R^2(x')dx' \\ & + s[(c_L^2 c_R^* + |c_L|^2 c_R)\phi_L + (c_L^* c_R^2 + c_L |c_R|^2)\phi_R] \int R(x-x')\phi_L(x')\phi_R(x')dx' \\ & + \delta|c_L|^4(c_L\phi_L + c_R\phi_R) \int R_2(x-x')\phi_L^4(x')dx' + \delta|c_R|^4(c_L\phi_L + c_R\phi_R) \int R_2(x-x')\phi_R^4(x')dx' \\ & + \delta \left[ (4|c_L|^4|c_R|^4 c_L + c_L^3 c_R^{*2} + c_L^* |c_L|^2 c_R^2)\phi_L + (4|c_L|^4|c_R|^4 c_R + c_R^3 c_L^{*2} + c_R^* |c_R|^2 c_L^2)\phi_R \right] \cdot \\ & \cdot \int R_2(x-x')\phi_L^2(x')\phi_R^2(x')dx' \\ & + 2\delta \left[ (|c_L|^2 c_L^2 c_R^* + |c_L|^4 c_R)\phi_L + (|c_L|^2 |c_R|^2 c_L + |c_L|^2 c_R^2 c_L^*)\phi_R \right] \int R_2(x-x')\phi_L^3(x')\phi_R(x')dx' \\ & + 2\delta \left[ (c_L^2 |c_R|^2 c_R^* + |c_L|^2 |c_R|^2 c_R)\phi_L + (|c_R|^4 c_L + c_R^2 |c_R|^2 c_L^*)\phi_R \right] \int R_2(x-x')\phi_R^3(x')\phi_L(x')dx'. \end{aligned}$$

In order to project the above equation onto the states  $\phi_{L,R}$  we multiply with the respective function (notice that the eigenfunctions are real due to the Hermitian nature of the operator  $\mathcal{L}$ ) and integrate. This involves the following integrals which will play a fundamental role in our considerations below:

$$\begin{aligned}\eta_0 &= \int \int R_1(x-x') \phi_L^2(x') \phi_L^2(x) dx' dx, \\ \eta_1 &= \int \int R_1(x-x') \phi_L^2(x') \phi_R^2(x) dx' dx, \\ \eta_2 &= \int \int R_1(x-x') \phi_L^2(x') \phi_L(x) \phi_R(x) dx' dx, \\ \eta_3 &= \int \int R_1(x-x') \phi_L(x') \phi_R(x') \phi_L(x) \phi_R(x) dx' dx,\end{aligned}$$

from the first nonlocal term, as well as

$$\begin{aligned}\eta_4 &= \int \int R_2(x-x') \phi_L^4(x') \phi_L^2(x) dx' dx, & \eta_8 &= \int \int R_2(x-x') \phi_L^2(x') \phi_R^2(x') \phi_L(x) \phi_R(x) dx' dx, \\ \eta_5 &= \int \int R_2(x-x') \phi_L^4(x') \phi_R^2(x) dx' dx, & \eta_9 &= \int \int R_2(x-x') \phi_L^3(x') \phi_R(x') \phi_L^2(x) dx' dx, \\ \eta_6 &= \int \int R_2(x-x') \phi_L^4(x') \phi_L(x) \phi_R(x) dx' dx, & \eta_{10} &= \int \int R_2(x-x') \phi_L^3(x') \phi_R(x') \phi_R^2(x) dx' dx, \\ \eta_7 &= \int \int R_2(x-x') \phi_L^2(x') \phi_R^2(x') \phi_L^2(x) dx' dx, & \eta_{11} &= \int \int R_2(x-x') \phi_L^3(x') \phi_R(x') \phi_L(x) \phi_R(x) dx' dx\end{aligned}$$

from the second nonlocal term. Some alternatives that are derived if we interchange the variables  $x$  and  $x'$  or swap  $L$  and  $R$  can also be equivalently considered. A numerical study of the first four integrals was already conducted in [34], where it was found that typically the integrals  $\eta_{2,3}$  can be considered as negligible in comparison to  $\eta_0$  which is the dominant term. On the other hand,  $\eta_1$  is close to  $\eta_{2,3}$  for near-local interactions (i.e., for small values of  $\sigma$ ), but becomes comparable to  $\eta_0$  as the latter decreases for wide nonlocal interaction ranges (i.e., for large  $\sigma$ ). The criterion that we use to determine whether  $\eta_1$  is negligible or not was  $\eta_{rel} \geq 0.01$  where  $\eta_{rel} = \eta_1 - \max(|\eta_2|, |\eta_3|)$ . This yields that  $\eta_1$  remains significant until (i.e., down to) a critical value  $\sigma_b = 2.96$  and  $1.56$  for the Gaussian and exponential kernels, respectively. The dependence of the relevant overlap integrals on the range of the interaction  $\sigma$  is shown in Fig. 2.

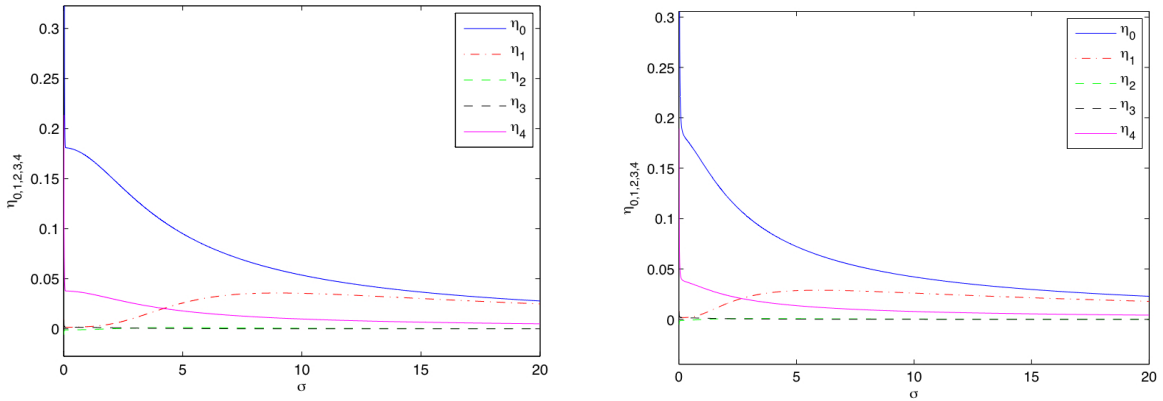


FIG. 2: The overlap integrals  $\eta_0$ ,  $\eta_1$ ,  $\eta_2$ ,  $\eta_3$  and  $\eta_4$  are shown as a function of the interaction range  $\sigma$  for the Gaussian (left) and exponential (right) kernels.

Taking into regard the second nonlocal term (which for simplicity we have assumed to share the same range parameter as the first), we can see from Fig. 3 that the integrals  $\eta_{5,6,\dots}$  are always negligible but  $\eta_4$  appears to be a nontrivial competing term. This is to a certain degree intuitively anticipated, as this represents the dominant term associated with the quintic interaction. Adapting the same criterion as in [34] (namely  $\eta_{rel} = \eta_4 - \max(|\eta_2|, |\eta_3|)$ ), we incorporate the relevant  $\eta_4$  for  $\sigma < \sigma_c = 9.15, 7.01$  for the Gaussian and exponential kernel, respectively. According to this we may distinguish three cases:

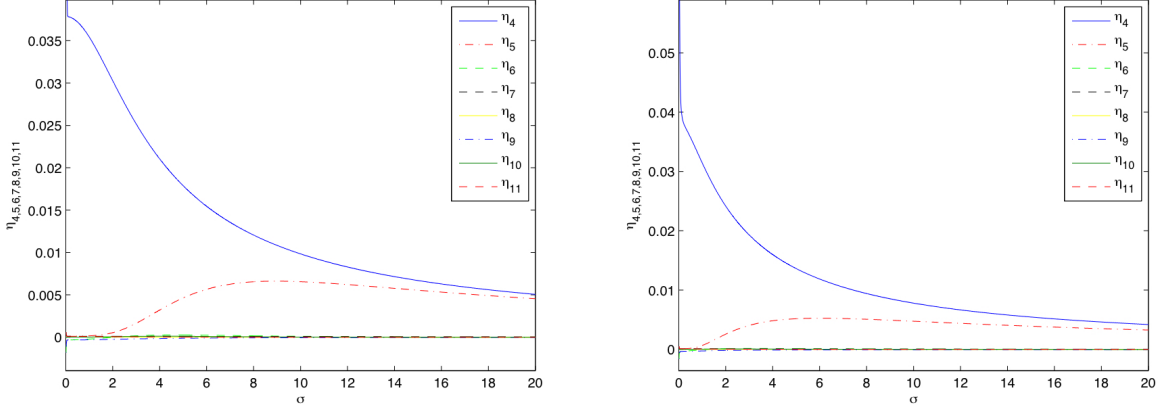


FIG. 3: The overlap integrals  $\eta_{4,5,\dots,11}$  are given here as a function of the interaction range  $\sigma$ , for the two kernels in order to appreciate the dominance of  $\eta_4$  with respect to the remaining terms for the range  $\sigma < \sigma_c$ , where the term with prefactor  $\eta_4$  is not negligible with respect to the overall dominant term  $\eta_0$ .

- The terms  $\eta_0$  and  $\eta_4$  are considered for  $\sigma < \sigma_b = 2.96$  (for the Gaussian kernel);
- The term with prefactor  $\eta_1$  is added when  $\sigma_b < \sigma < \sigma_c$ .
- For  $\sigma > \sigma_c$ ,  $\eta_4$  is omitted and only  $\eta_0$ ,  $\eta_1$  are taken into account.

For the first case, the projection of the equation onto the states  $\phi_{L,R}$  yields

$$\begin{aligned} i\dot{c}_L &= (\Omega - \mu)c_L - \omega c_R + s\eta_0|c_L|^2 c_L + \delta\eta_4|c_L|^4 c_L \\ i\dot{c}_R &= (\Omega - \mu)c_R - \omega c_L + s\eta_0|c_R|^2 c_R + \delta\eta_4|c_R|^4 c_R, \end{aligned}$$

and by introducing Madelung representation of action-angle or amplitude-phase decomposition ( $c_{L,R} = \rho_{L,R}e^{i\theta_{L,R}}$ ), we obtain

$$\left\{ \begin{array}{l} \dot{\rho}_L = \omega \rho_R \sin \theta \\ \dot{\theta}_L = \mu - \Omega + \omega \frac{\rho_R}{\rho_L} \cos \theta - s\eta_0 \rho_L^2 - \delta\eta_4 \rho_L^4, \end{array} \right\} \quad (3)$$

where we have defined the relative phase  $\theta = \theta_L - \theta_R$  and the respective equations for  $\rho_R$  and  $\theta_R$  can be obtained by exchanging  $L$  and  $R$  and using  $-\theta$  instead of  $\theta$ . Focusing now on the steady solutions (satisfying  $\dot{\rho}_{L,R} = \dot{\theta}_{L,R} = 0$ ), we need to enforce  $\theta = 0$  or  $\pi$  for non-zero amplitudes. This leads us to symmetric and antisymmetric (equal or opposite amplitudes) *pairs* of solutions, namely for  $\theta = 0$  we have the symmetric (only positive ones among the) solutions  $\rho_{L,R}^2 = \left(-s\eta_0 \pm \sqrt{\eta_0^2 - 4\delta\eta_4(\omega_0 - \mu)}\right) / 2\delta\eta_4$  with  $\mu < \omega_0 + \frac{\eta_0^2}{4\eta_4}$ , for  $\delta = -1$  ( $\mu > \omega_0 - \frac{\eta_0^2}{4\eta_4}$  for  $\delta = 1$ ). Also, for  $\theta = \pi$ , we have (only the positive amplitude ones among) the antisymmetric solutions  $\rho_{L,R}^2 = \left(-s\eta_0 \pm \sqrt{\eta_0^2 - 4\delta\eta_4(\omega_1 - \mu)}\right) / 2\delta\eta_4$  with  $\mu < \omega_1 + \frac{\eta_0^2}{4\eta_4}$  for  $\delta = -1$  (resp.  $\mu > \omega_1 - \frac{\eta_0^2}{4\eta_4}$  for  $\delta = 1$ ). For the asymmetric solutions one has to solve the polynomial

$$\delta\eta_4 \rho_{L,R}^6 + s\eta_0 \rho_{L,R}^4 + (\Omega - \mu) \rho_{L,R}^2 + \frac{\omega^2}{s\eta_0 + \delta\eta_4 N} = 0,$$

which can more conveniently be written as a function of the norm of the solutions (representing the atom number in BECs and the optical intensity in optics). Thus, introducing  $N$  ( $N = \rho_L^2 + \rho_R^2$ ) yields the quartic polynomial

$$\delta^3 \eta_4^3 N^4 + 3s\eta_4^2 \eta_0 N^3 + (3\delta\eta_4 \eta_0^2 - \eta_4^2(\mu - \Omega))N^2 + (s^3 \eta_0^3 - 2s\delta\eta_0 \eta_4(\mu - \Omega))N - \delta\eta_4 \omega^2 - \eta_0^2(\mu - \Omega) = 0.$$

For the second case ( $\sigma > \sigma_b$ ) the integrals  $\eta_0$ ,  $\eta_1$ ,  $\eta_4$  are taken into account and the projection equations onto the states  $\phi_{L,R}$ , read:

$$\begin{aligned} i\dot{c}_L &= (\Omega - \mu)c_L - \omega c_R + s c_L(\eta_0|c_L|^2 + \eta_1|c_R|^2) + \delta\eta_4|c_L|^4 c_L \\ i\dot{c}_R &= (\Omega - \mu)c_R - \omega c_L + s c_R(\eta_0|c_R|^2 + \eta_1|c_L|^2) + \delta\eta_4|c_R|^4 c_R. \end{aligned}$$

Here, the amplitude-phase decomposition yields

$$\left\{ \begin{array}{l} \dot{\rho}_L = \omega \rho_R \sin \theta \\ \dot{\theta}_L = \mu - \Omega + \omega \frac{\rho_R}{\rho_L} \cos \theta - s\eta_0 \rho_L^2 - s\eta_1 \rho_R^2 - \delta\eta_4 \rho_L^4. \end{array} \right\}$$

We can, once again, obtain the set of stationary solutions as follows. When  $\theta = 0$  (symmetric case) the solutions will be (the positive amplitude ones among)  $\rho_{L,R}^2 = \left( -s(\eta_0 + \eta_1) \pm \sqrt{(\eta_0 + \eta_1)^2 - 4\delta\eta_4(\omega_0 - \mu)} \right) / 2\delta\eta_4$  for  $\mu < \omega_0 + \frac{(\eta_0 + \eta_1)^2}{4\eta_4}$  for  $\delta = -1$  ( $\mu > \omega_0 - \frac{(\eta_0 + \eta_1)^2}{4\eta_4}$  for  $\delta = 1$ ) and when  $\theta = \pi$  (antisymmetric case) the solutions are (the positive amplitude ones among)  $\rho_{L,R}^2 = \left( -s(\eta_0 + \eta_1) \pm \sqrt{(\eta_0 + \eta_1)^2 - 4\delta\eta_4(\omega_1 - \mu)} \right) / 2\delta\eta_4$  and exist for  $\mu < \omega_1 + \frac{(\eta_0 + \eta_1)^2}{4\eta_4}$  for  $\delta = -1$  ( $\mu > \omega_1 - \frac{(\eta_0 + \eta_1)^2}{4\eta_4}$  for  $\delta = 1$ ). The asymmetric solutions now, directly in norm expression, will be given by the polynomial

$$\begin{aligned} \delta^3 \eta_4^3 N^4 &+ (3s\eta_4^2 \eta - s\eta_4^2 \eta_1) N^3 + (3\delta\eta_4 \eta^2 - \eta_4^2(\mu - \Omega) - 2\delta\eta_4 \eta \eta_1) N^2 + \\ &+ (s^3 \eta^3 - 2s\delta\eta \eta_4(\mu - \Omega) - s\eta_1 \eta_4^2) N - \delta\eta_4 \omega^2 - \eta^2(\mu - \Omega) = 0 \end{aligned}$$

with  $\eta$  here standing for  $\Delta\eta = \eta_0 - \eta_1$ .

In the third case, when  $\sigma > \sigma_c$ , the effect of the quintic terms is deemed to be negligible and the situation reverts to the analysis of [34] and is hence omitted here.

## B. The bifurcation analysis

In order to derive a more convenient form of the system so that we can proceed to the analysis of the spontaneous symmetry breaking (SSB) bifurcation, we introduce the population imbalance between the two wells,

$$z = (N_L - N_R)/N = (|c_L|^2 - |c_R|^2)/N, \quad (4)$$

where  $N_{L,R} = |c_{L,R}|^2 = \rho_{L,R}^2$  and  $N = N_L + N_R$ . Together with the relative phase between the two wells  $\theta = \theta_L - \theta_R$ , this forms a set of conjugate variables, in which we obtain the dynamical system :

$$\left\{ \begin{array}{l} \dot{z} = 2\omega\sqrt{1-z^2} \sin \theta \\ \dot{\theta} = -\frac{2\omega z \cos \theta}{\sqrt{1-z^2}} - s\eta N z - \delta\eta_4 N^2 z. \end{array} \right\}$$

This can be written in the Hamiltonian form

$$\left\{ \begin{array}{l} \dot{z} = -\frac{\partial \mathcal{H}}{\partial \theta} \\ \dot{\theta} = \frac{\partial \mathcal{H}}{\partial z} \end{array} \right\} \quad (5)$$

with the Hamiltonian function

$$\mathcal{H} = 2\omega\sqrt{1-z^2} \cos \theta - \frac{1}{2}s\eta N z^2 - \frac{1}{2}\delta\eta_4 N^2 z^2.$$

Note that  $\eta$  stands either for  $\eta_0$  ( $\sigma < \sigma_b$ ) or for  $\Delta\eta = \eta_0 - \eta_1$  ( $\sigma_b < \sigma < \sigma_c$ ). The system possesses the stationary solutions (critical points)  $(z_1, \theta_1)$  and  $(z_2, \theta_2)$  with  $z_1 = z_2 = 0$ ,  $\theta_1 = 0$ ,  $\theta_2 = \pi$  that correspond to the symmetric

and antisymmetric solutions, identified above. Furthermore, the stationary solutions representing the asymmetric branches are given by:

$$z^2 = 1 - \frac{4\omega^2}{(s\eta N + \delta\eta_4 N^2)^2}, \quad \theta = 0, \pi.$$

These branches emerge and merge as bifurcations from and to the symmetric or antisymmetric solutions and they exist for those values of  $N$  for which  $z^2 \geq 0$ . Taking  $z = 0$ , we get that

$$N = (-s\eta \pm \sqrt{\eta^2 + 8\delta\eta_4\omega})/2\delta\eta_4, \quad N = (-s\eta \pm \sqrt{\eta^2 - 8\delta\eta_4\omega})/2\delta\eta_4. \quad (6)$$

By substituting  $(s, \delta) = (1, -1)$  or  $(-1, 1)$  we get the same four possible expressions for  $N$  as a function of  $\sigma$  that are displayed in fig.4 and we denote them with  $N_0^{cr}$ ,  $N_1^{cr}$ ,  $N_2^{cr}$  and  $N_3^{cr}$  (the subscripts 0 and 2 correspond to the  $(-)$  signs in the left and right expressions of Eq. (6), respectively, while the subscripts 1 and 3 to the  $(+)$  signs). One can then see that when  $(s, \delta) = (1, -1)$  and demanding that  $z^2 > 0$ , one gets that  $N$  should either lie in the area outside the curves  $N_0^{cr}$  and  $N_1^{cr}$  or in the area inside the curves  $N_2^{cr}$  and  $N_3^{cr}$ . In the case of  $s = -1$  and  $\delta = 1$ , the role of the symmetric and anti-symmetric branches gets exchanged in as far as the bifurcation of the asymmetric branch is concerned (see also below).

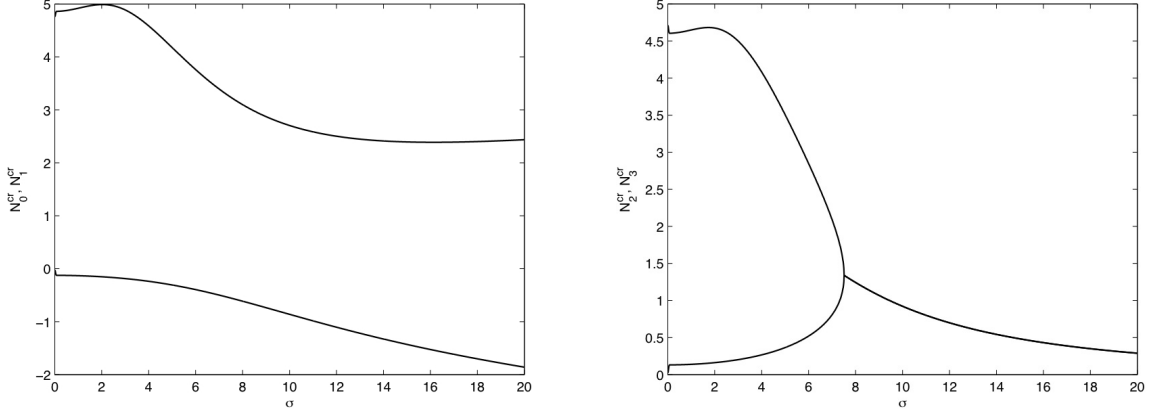


FIG. 4: The critical values  $N_0^{cr}$ ,  $N_1^{cr}$  (left panel) and  $N_2^{cr}$ ,  $N_3^{cr}$  (right panel) whenever  $(s, \delta) = (1, -1)$  show when the bifurcations appear. More specifically, the left panel corresponds to the bifurcations that occur on the symmetric branch and the right panel for those that occur on the antisymmetric one.

Importantly, it can be observed in Fig. 4 that  $N_0^{cr}$  is always negative, hence it is omitted for the principal case considered herein, namely  $s = 1$  and  $\delta = -1$ . On the one hand, the *critical* conclusion of our analysis is that for  $\sigma < 7.52$ , the system is predicted to have for the anti-symmetric branch both a symmetry breaking bifurcation (at  $N = N_2^{cr}$ ) and a symmetry restoring one that eliminates the asymmetric branch (at  $N = N_3^{cr}$ ). On the other hand, the right panel suggests that  $N_2^{cr}$ ,  $N_3^{cr}$  coincide  $\sigma \geq 7.52$ , beyond which there is only a single (symmetry breaking) bifurcation. However, as will be discussed below, for large interaction range  $\sigma$  this prediction seems to have some discrepancy from what actually happens as we will see that in fact, we observe a symmetry restoring bifurcation while we do not observe a bifurcation at all in the symmetric branch. To the best of our knowledge, this is the first example of an analytical prediction of the existence of a symmetry restoring bifurcation, a feature that is unique to the analysis of the normal form of the bifurcation for the cubic-quintic case (and cannot be predicted e.g. in the purely cubic case two-mode analysis of [34]). The new critical points appear or disappear as a pitchfork bifurcation that emerges from the antisymmetric solutions for  $\theta = \pi$  respectively. From the symmetric solution, in this case of  $s = 1$  and  $\delta = -1$ , only a single bifurcation arises at  $N = N_1^{cr}$ .

For the opposite case (to the one principally considered herein) of  $s = -1$  and  $\delta = 1$ , i.e., for a focusing cubic nonlinearity, the bifurcations emerge from the symmetric branch, while for  $s = 1$ , i.e., for a defocusing cubic term, then the relevant symmetry breakings arose from the anti-symmetric branch. Thus, in this case, we expect an asymmetric branch to bifurcate and break the symmetry at  $N = N_2^{cr}$ , while it returns to the parent symmetric branch restoring the symmetry at  $N = N_3^{cr}$ . On the other hand, for the anti-symmetric waveform with a focusing cubic nonlinearity, only a single bifurcation arises at  $N = N_1^{cr}$ . We provide further details of each of these bifurcations and their comparison with the full numerics of the underlying NLS model in the next section.

From the system of Eqs. (5), one can reduce the dynamical evolution to a single second-order ODE:

$$\ddot{z} = -4\omega^2 z - (s\eta Nz + \delta\eta_4 N^2 z)\sqrt{4\omega^2 - 4\omega^2 z^2 - \dot{z}^2}$$

which can also be rewritten in the “position-momentum” variables as:

$$\begin{cases} \dot{z} = p, \\ \dot{p} = -4\omega^2 z - (s\eta Nz + \delta\eta_4 N^2 z)\sqrt{4\omega^2 - 4\omega^2 z^2 - p^2}. \end{cases} \quad (7)$$

This renders the system amenable to the phase plane representation of the form shown in Fig. 5. Here we observe that there is a stationary solution  $\dot{z} = \dot{p} = 0$  which is a fixed point of the center type. However, for the cases when  $(s, \delta) = (1, -1)$ , for  $N$  crossing the critical point  $N_1^{cr}$  in the case of the symmetric branch and for  $N \in [N_2^{cr}, N_3^{cr}]$  in the case of the anti-symmetric branch, there appear two more critical points at  $p = 0$  and  $z = \pm\sqrt{1 - \frac{4\omega^2}{(s\eta N + \delta\eta_4 N^2)^2}}$ , representing the asymmetric solutions. The point  $(0,0)$  is a fixed point of center type before the bifurcation occurs, but past the relevant critical number of atoms (or optical intensity), it becomes a saddle as the two new (asymmetric) fixed points that appear are of center type. Fig. 5 shows the phase space of the full system, as well as the vicinity of the critical points for the Gaussian kernel with  $\sigma = 1$ ,  $N_1^{cr} = 4.9862$  and  $N = 5$ .

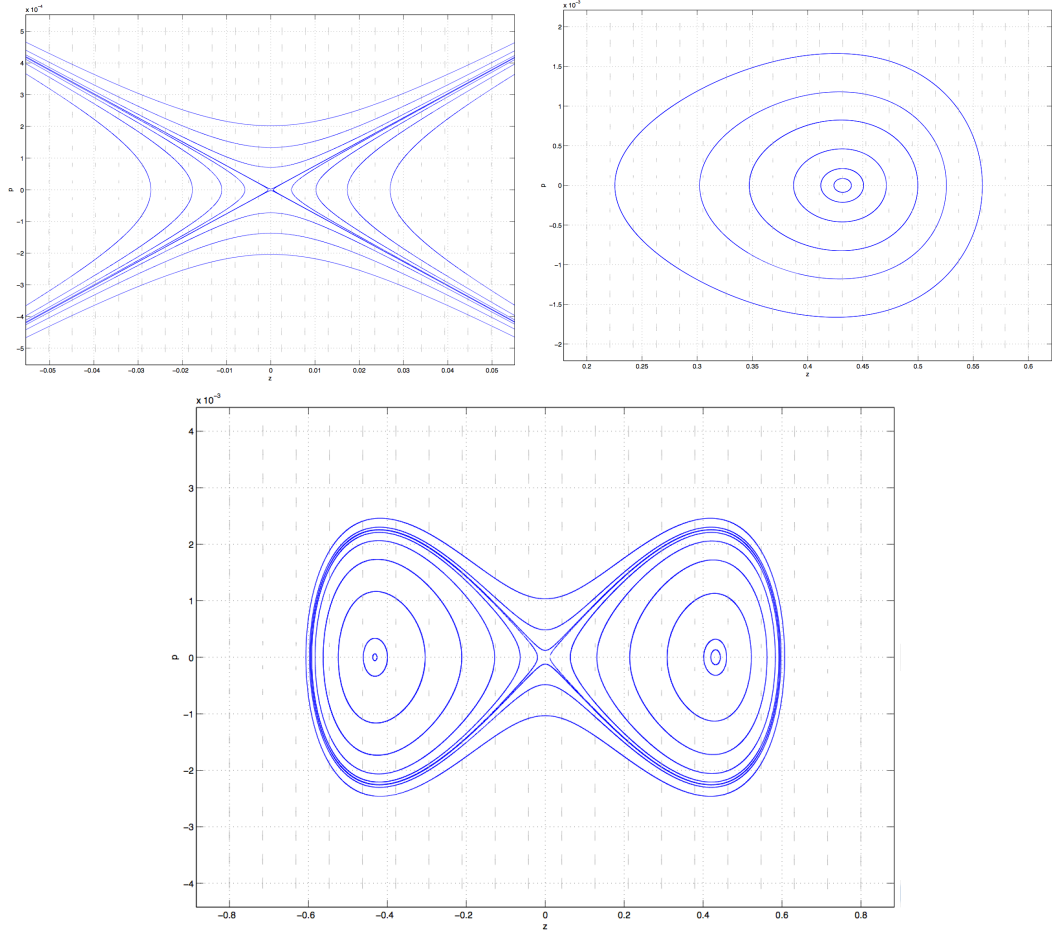


FIG. 5: Top panels: The phase space diagrams of the Hamiltonian system when  $s = 1$  and  $\delta = -1$  with the Gaussian kernel, for  $\sigma = 1$ ,  $N = 5$ , and with  $N_1^{cr} = 4.9862$  (after the new fixed points are created at  $(\pm 0.4318, 0)$ ). The left panel displays the region of phase space near the symmetric solution  $(0,0)$  (saddle) and the right panel the one near one of the asymmetric fixed points  $(0.4318, 0)$  (center). The bottom panel shows the full phase space diagram of the system for  $N = 5$ .



### III. NUMERICAL APPROACH

#### A. Stationary solutions

We now turn to the examination of our analysis against the results of numerical bifurcation analysis (and in the next subsection also compare them to direct numerical simulations). We focus here on the case where  $s = 1$ ,  $\delta = -1$ , as we are especially interested in the case of *competing* interactions; we will briefly also touch upon the case of  $s = -1$  and  $\delta = 1$ . In our numerical computations, the stationary solutions are obtained by using a fixed-point Newton-Raphson iteration for a finite difference decomposition of the relevant boundary value problem, with a choice of the grid spacing of  $\Delta x = 0.1$  and employing a parametric (and wherever needed a pseudo-arclength) continuation of the solutions with respect to the chemical potential parameter  $\mu$  (in optics this is the so-called propagation constant). The linear stability is analyzed by considering the standard linearization around the stationary solutions  $\psi_0$  in the form

$$\psi(x, t) = \psi_0 + \epsilon(a(x)e^{\lambda t} + b^*(x)e^{\lambda^* t}).$$

This yields the eigenvalue problem

$$\begin{pmatrix} L_1 & L_2 \\ -L_2^* & -L_1^* \end{pmatrix} \begin{pmatrix} a \\ b \end{pmatrix} = i\lambda \begin{pmatrix} a \\ b \end{pmatrix},$$

where the operators are defined as

$$\begin{aligned} L_1\phi = & \left[ -\frac{1}{2}\partial_x^2 + V - \mu + s \int_{-\infty}^{+\infty} K(x-x')|\psi_0(x')|^2 dx' + \delta \int_{-\infty}^{+\infty} K(x-x')|\psi_0(x')|^4 dx' \right] \phi + \\ & + s \int_{-\infty}^{+\infty} K(x-x')\psi_0(x)\psi_0^*(x')\phi(x')dx' + 2\delta \int_{-\infty}^{+\infty} K(x-x')\psi_0(x)\psi_0(x')\psi_0^{*2}(x')\phi(x')dx' \end{aligned}$$

and

$$L_2\phi = s \int_{-\infty}^{+\infty} K(x-x')\psi_0(x')\psi_0(x)\phi(x')dx + 2\delta \int_{-\infty}^{+\infty} K(x-x')\psi_0(x)\psi_0^*(x')\psi_0^2(x')\phi(x')dx'$$

for any real function  $\phi$ . Instability is guaranteed by the existence of any eigenvalues  $\lambda$  of the linearized operator with  $\Re(\lambda) \neq 0$  in the sense that perturbations along the corresponding eigendirections will deviate exponentially from the corresponding fixed point. Recall that this is also the case for all eigenvalues of our Hamiltonian system, since when  $\lambda$  is an eigenvalue, so are  $-\lambda$ ,  $\lambda^*$  and  $-\lambda^*$ . In the case where all eigenvalues are found to be purely imaginary, then the solution is found to be marginally stable.

In our specific case of competing interactions, we comment on the following. The positive value ( $s = 1$ ) denotes the repulsive behavior of the cubic nonlocal term while the negative one  $\delta = -1$  leads to attractive behavior of the quintic nonlocal nonlinearity. As we examine the bifurcation problem of nonlinear states from the corresponding linear eigenstates, we expect that for lower values of  $N$  (i.e., weaker nonlinearities), the former repulsive term should be dominant, while for larger values of  $N$  (i.e., stronger nonlinearities), it is anticipated that the latter attractive term will take over. This is accurately reflected in the numerical bifurcation diagrams that we now show in Figs. 6-8, for three (distinct by roughly an order of magnitude in each case) values of the range  $\sigma$ . The first value of  $\sigma = 0.1$  in Fig. 6 is supposed to reflect the local case (since the range of interaction is much smaller than any other intrinsic length scale in the system). Here the agreement with the two-mode approximation is very good quantitatively for low  $N$  and very good qualitatively (and even good quantitatively for some features such as chemical potentials of critical points) for large  $N$ . The quality of these types of agreements is found to be preserved for an intermediate interaction range of  $\sigma = 1$  in Fig. 7. However, when the interaction range becomes sufficiently large that it competes (or overcomes) the length scale of the potential wells, then fundamental disparities are expected to be found and that is the very conclusion of Fig. 8 for  $\sigma = 8$ .

In the first case where  $\sigma = 0.1$ , the symmetric and antisymmetric branches of nonlinear states emanate from  $\mu = 0.1328$  and  $0.1557$ , as expected, respectively ( $\omega_0$  and  $\omega_1$ ), both of them being dynamically stable, for sufficiently small values of  $N$ . The rightward bending of the branches for small  $N$  confirms the dominance of the self-repulsive part of the (cubic) interactions for small  $N$ , as indicated above. The antisymmetric branch (top right panel of Fig. 6 and see also the zoom of the bottom panel of the figure) is destabilized and the theoretically predicted asymmetric branch emerges. The numerical value of the chemical potential for the bifurcation point is found to be  $\mu = 0.1686$ , whereas the corresponding analytical one is  $\mu = 0.1679$ , confirming the quantitative nature of the agreement with the

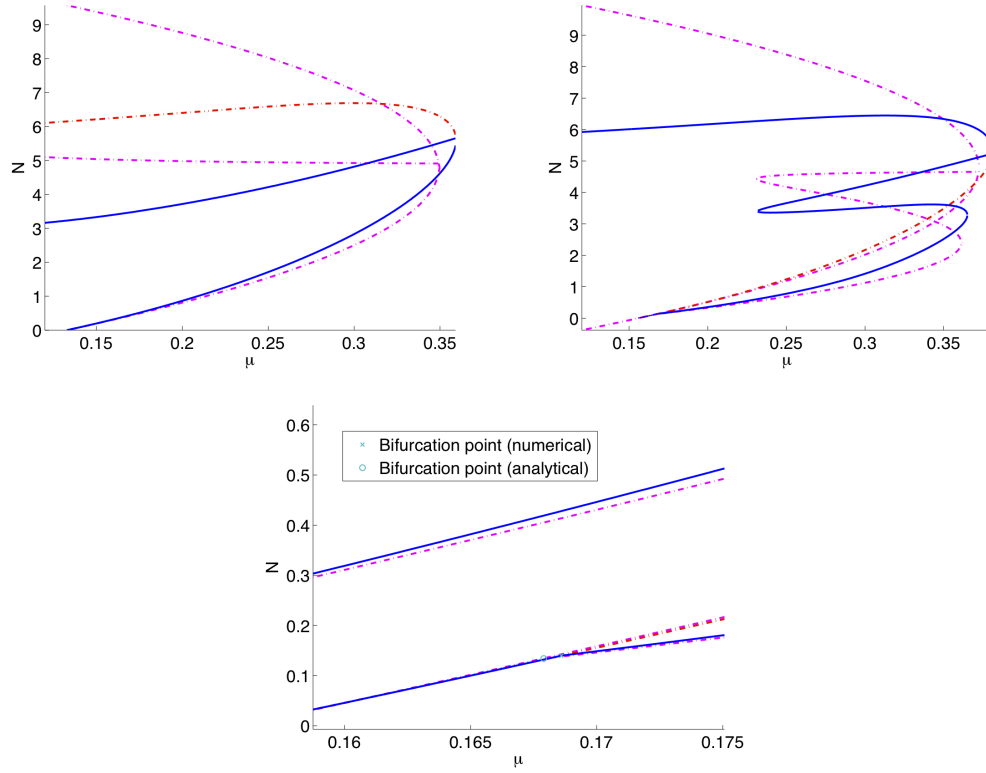


FIG. 6: The stationary solution branches for the case  $s = 1$ ,  $\delta = -1$  when the interaction range is  $\sigma = 0.1$  expressed in terms of the normalized  $N$  as a function of  $\mu$ . The analytical predictions are denoted with the purple dash-dotted line while the numerically determined solutions are denoted with the solid line that is blue when it is stable and red otherwise. The top left panel shows the symmetric solutions, while the top right presents the antisymmetric ones, both including the asymmetric bifurcations that emerge from them. The bottom panel presents a detail of the symmetry-breaking effect, showcasing the quality of its approximation by the two-mode expansion.

two-mode approximation. For larger  $N$ , we observe that the asymmetric solution has two apparent turning points (where the sign of  $dN/d\mu$  changes, but in fact its stability does not change), before it reaches the anti-symmetric branch at the numerically computed value  $\mu = 0.381$  where we observe the symmetry restoring effect, which, in fact, re-stabilizes the anti-symmetric branch. In our theoretical analysis, we observe the same qualitative behavior and the symmetry restoring occurs at  $\mu = 0.3723$ , in reasonable agreement with the full numerical results. Two additional observations should be made here. On the one hand, since the symmetry restoring occurs at much larger values of  $N$ , the relevant agreement is expected to be less adequate quantitatively than for the symmetry breaking occurring at lower  $N$ . This is because a two-mode expansion is less appropriate of a reduction at such higher nonlinearities. On the other hand, it can indeed be observed that while the overall trend of the two curves is the same (and even critical/turning points in terms of their chemical potential are rather accurately captured), this agreement is not adequate quantitatively e.g. for critical values of  $N$  (or for detailed quantitative matching of the curves for large  $N$ ). For the symmetric solution of the top left panel of Fig. 6, we can observe that it is increasing monotonically until  $\mu = 0.359$  where it sustains a pitchfork bifurcation leading to the emergence of an asymmetric branch and also a subsequent turning point. The symmetric branch becomes unstable thereafter and the asymmetric emerging state is the stable daughter branch. Notice that the theoretical analysis is once again quantitatively accurate for small  $N$  and the agreement becomes more qualitative for higher  $N$ 's. The critical point for the emergence of the asymmetric branch is predicted for  $\mu = 0.3492$  in reasonable agreement with the full numerical result.

For the case of  $\sigma = 1$  the effects are similar to those in the previous case. The symmetry breaking of the antisymmetric branch (top right, as well as zoom in of the bottom panel of Fig. 7) occurs now at  $\mu = 0.168$  according to the numerical results and at  $\mu = 0.1673$  in the two-mode approximation, again attesting to its validity for small  $N$ . After following a similar trajectory with the case  $\sigma = 0.1$ , the asymmetric solution merges back to the antisymmetric one at  $\mu = 0.374$  (numerical value) or at  $\mu = 0.364$  (analytical value) with the antisymmetric branch again regaining its stability past the symmetry restoring bifurcation. The symmetric solution (top left panel of Fig. 7) again increases

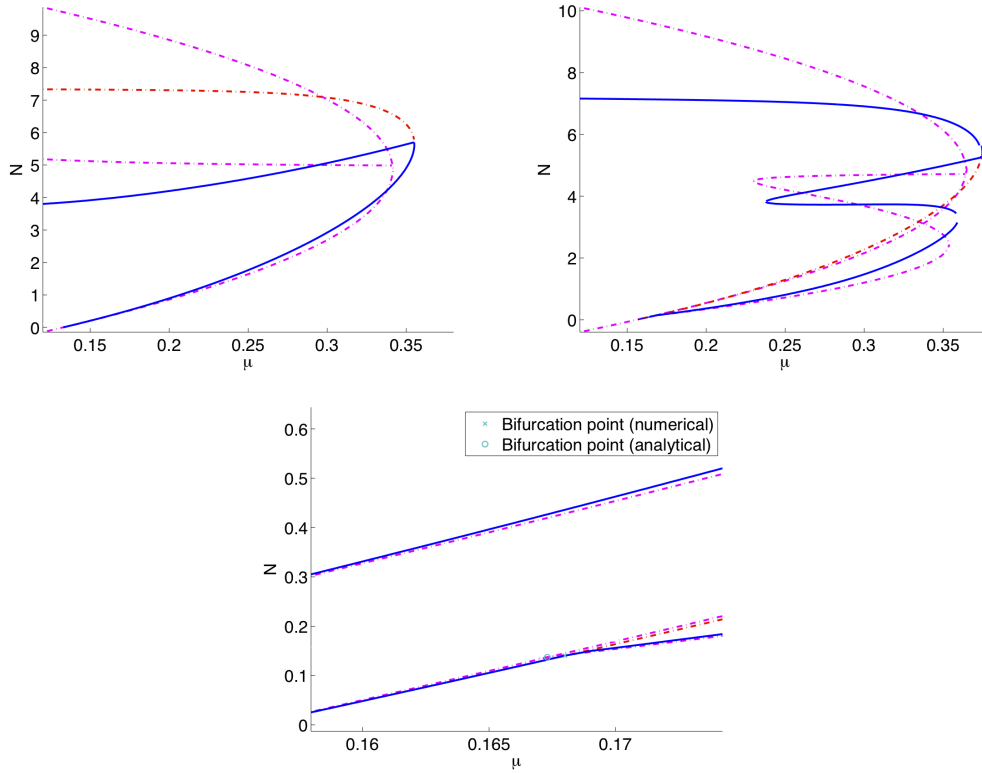


FIG. 7: This figure shows the same features as the previous one for the symmetric branch (top left panel), the anti-symmetric branch (top right panel) and a zoom-in of the symmetry breaking (bottom panel). However, the interaction range here is an order of magnitude larger, namely  $\sigma = 1$ .

monotonically until it sustains a symmetry breaking bifurcation of its own at  $\mu = 0.355$ . The two-mode approximation predicts this bifurcation to arise at  $\mu = 0.342$ .

Next, in Fig. 8, we increase the interaction range, roughly, another order of magnitude by setting  $\sigma = 8$ . Here, as may be intuitively expected given that the interaction range is wider than the wells of the potential, the results are quite different. For small values of  $\mu$  (and thus atom number  $N$  or optical power) we have a quite satisfactory agreement (even quantitative) with the two mode approximation, as may be expected. As a demonstration of that, we note that the symmetry breaking of the antisymmetric branch occurs in our analysis at  $\mu = 0.1981$ , while numerically it is found to take place at  $\mu = 0.195$ . On the other hand, due to the predicted earlier collision of the critical points  $N_2^{cr}$  and  $N_3^{cr}$ , there is no symmetry restoring taking place in our normal form reduction. Nevertheless, we observe that such a restoring, in fact, still takes place in the full numerical bifurcation diagram. Furthermore, in this case, we have not been able to detect a symmetry-breaking bifurcation in the case of the symmetric branch, even though such a bifurcation is predicted within the reduction. This illustrates that for such large values of  $\sigma$ , even the qualitative agreement previously associated with the large  $N$  case dynamics should not be expected to be present.

Finally, we examine also one case where we switch the signs of the nonlocal terms to  $(s, \delta) = (-1, 1)$ , so now the cubic term is the one that behaves attractively while the quintic one behaves repulsively. This is illustrated in Fig. 9. The interaction range  $\sigma$  is selected here to be 1 and here we see that the same phenomenology appears in a region where the chemical potential varies from  $-0.08$  to  $0.155$ , thus attaining negative values. As earlier, both states emanate for the same values of  $\mu$  and as we decrease its value we observe the symmetry breaking at  $\mu = 0.1212$  (both for numerical and analytical) this time on the symmetric state which becomes unstable. As we further decrease the chemical potential to negative values of  $\mu$ , the symmetry restoring of the asymmetric state towards its parent symmetric branch occurs at  $\mu = -0.0727$  (numerical value). The analytical prediction for this critical point is  $\mu = -0.0755$ . Hence, once again we observe a good qualitative agreement for larger  $N$  (although once again slight quantitative disparities exist between the overall curves and the critical points in terms of  $N$ ). A look at the antisymmetric branch now shows us that a bifurcation occurs at the point where the solution changes slope ( $dN/d\mu$ ), precisely at  $\mu = -0.0465$  (numerical) and is theoretically predicted to arise at  $\mu = -0.0526$  (analytical) with the antisymmetric branch becoming unstable past this

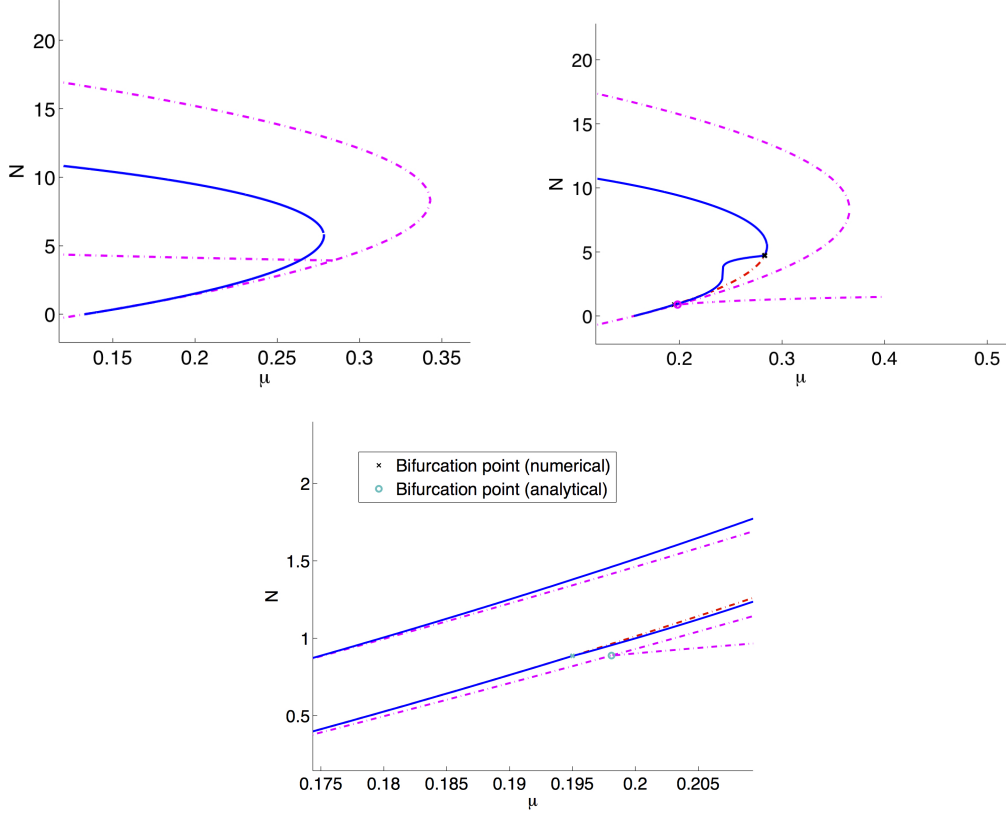


FIG. 8: Same as the previous two figures, but now for large nonlocality interaction range in the case of  $\sigma = 8$ .

critical point. Once again the zoom of the bottom panel confirms the quantitative nature of the analytical-numerical agreement for small values of  $N$ , which retains its qualitative value even for larger  $N$ .

## B. Dynamics

Finally, we briefly turn to the dynamics of the system, in order to observe the implications of the dynamical instability due to the symmetry breaking. The relevant evolution of the unstable solutions for  $\mu = 0.19$  and  $\mu = 0.25$ , in the case of  $\sigma = 1$  (recall that  $s = 1$  and  $\delta = -1$ ) are shown in Fig. 10. In both cases, it can be seen that the weak perturbation added on top of the exact numerical solution in the initial conditions has a projection along the unstable eigenmode. This projection, for sufficiently long times (about 200 in the left panel and about 100 in the right panel), gets amplified and eventually leads to a visible (i.e., of order unity) symmetry breaking in the profile of the state. While the space-time evolution of the density (in the atomic case; optical intensity in the optical case) is shown in Fig. 10, an interesting alternative way to visualize the instability was proposed recently by [37]. In the latter work, the PDE dynamics was, in fact, projected to the phase plane of the two-mode approximation and visualized therein. An example of such a visualization for the case of  $\mu = 0.19$  can be seen in Fig. 11. From both the phase plane curves and the profiles illustrated underneath of the solution at different times, we can extract some interesting conclusions. In particular, in the one degree of freedom reduction of our theoretical analysis, the trajectory occurs over iso-contours of the energy. Hence, the kind of phase plane picture shown in Fig. 11 would only be possible by “conglomerating” many distinct orbits. However, it is important to appreciate that the PDE has infinitely many degrees of freedom. In that capacity, it is possible for the “subspace” of our two-mode approximation to *dissipate* energy towards (or possibly regain energy from) higher energy states (of the point spectrum of the system). In so doing, it appears as if the system visits further and further inward trajectories of lower energy, because indeed the excess energy has been imparted to other degrees of freedom. This yields a clear illustration of how the subspace of our two-modes is a *closed system* for the ODE reduction, but instead is an *open system* for the full PDE evolutionary dynamics [41].

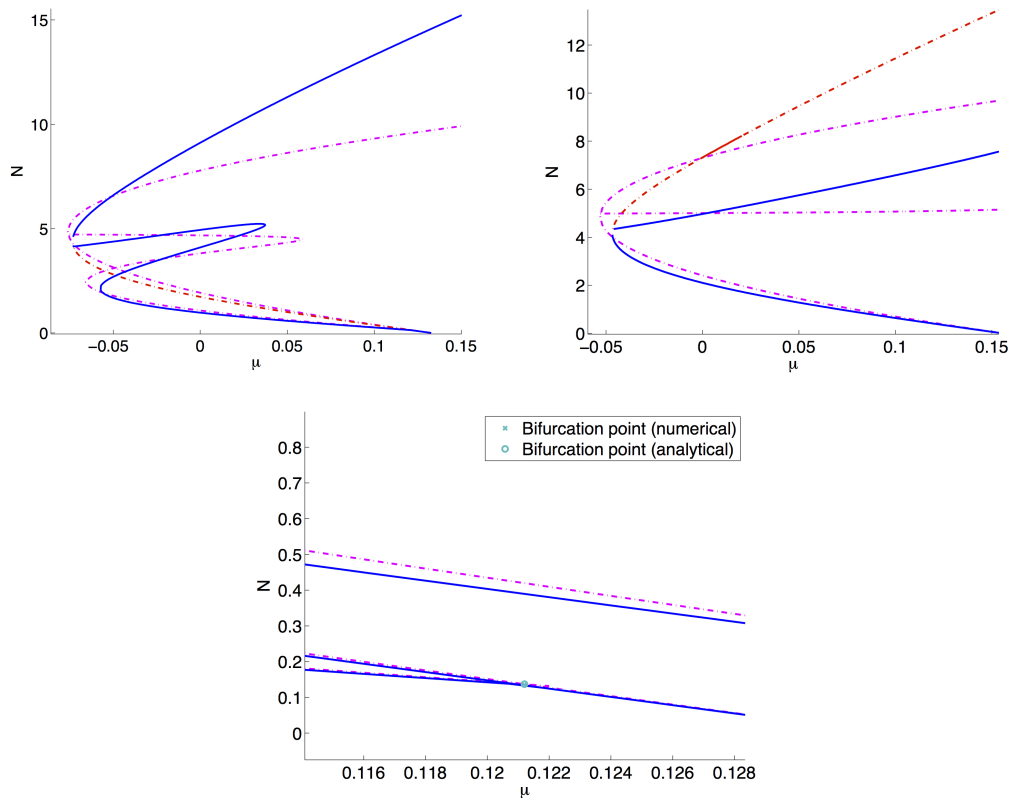


FIG. 9: Same as the previous three figures, but now for the *focusing cubic/defocusing quintic* case of  $s = -1$  and  $\delta = 1$ , for an intermediate interaction range of  $\sigma = 1$ .

#### IV. CONCLUSIONS

In the present work, we examined double well potentials in the presence of nonlocal interactions both in the cubic and in the quintic part of the nonlinearity. We attempted to address such settings by means of a two-mode decomposition that has the notable advantage that nonlocality is not substantially different to handle therein, as the nonlocal kernels merely contribute to relevant overlap integrals that need some systematic book-keeping, but are otherwise not considerably harder than is the locally nonlinear case. There are some particularly important attributes of the quintic case that we were able to extract via a normal form reduction and phase plane visualization (under suitable circumstances of “competition” e.g. for a defocusing cubic but focusing quintic nonlinearity). One such is that contrary to the purely cubic case, the reduction is able to predict not only a symmetry breaking bifurcation, but *also* a symmetry restoring one (at least for a suitable interval of range parameters for the interaction kernel). Another unusual characteristic is that symmetry breaking bifurcations are encountered *both* for the symmetric and the antisymmetric branch, again differently than is the case for the cubic nonlinearity in the double well setting. These features were tested against numerical bifurcation results and good agreement was found where appropriate (e.g. low atom numbers and a suitable range of the interaction range). Disparities arising for high  $N$  and large  $\sigma$  were systematically explained. Finally, the instability dynamics was visualized not only by space-time density evolution plots but also by offering its projection to the phase plane of the double well theoretical reduction and assessing the similarities and differences therein of the ODE approximation and full PDE result.

There are numerous possibilities for the extension of the present results to more elaborate contexts. On the one hand, even in the one-dimensional setting, one could envision a study of different interaction ranges between the cubic and quintic terms (or, for that matter, combinations of local and nonlocal nonlinearities within the cubic and/or quintic terms). On the other hand, extensions to one dimensional settings with more wells would bring along a richer phenomenology (in that setting the three-well local case has been studied [38] and was recently revisited in [39]), while in higher dimensional settings such as 2d, four well settings in a square configuration [40] or other configurations exploiting the geometry of the system would be interesting to study.

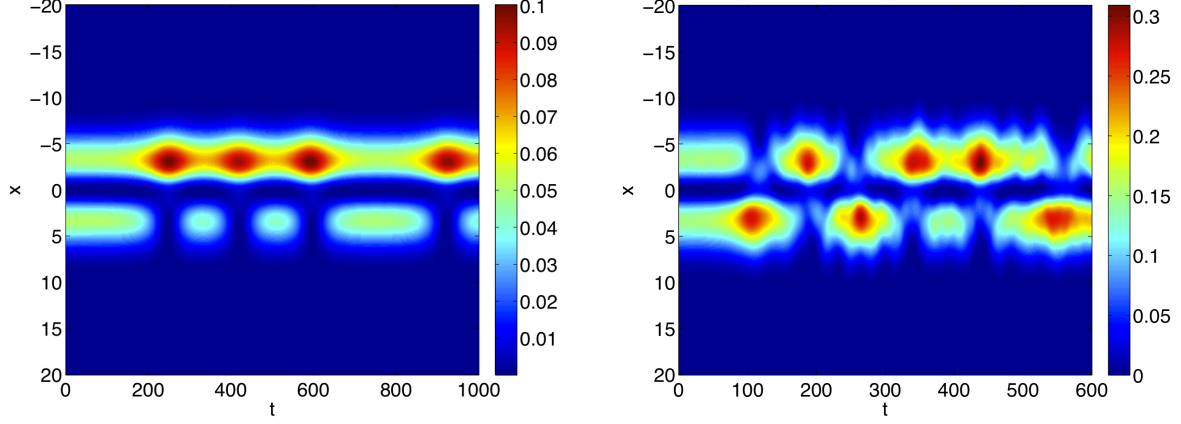


FIG. 10: Spatio-temporal contour plot of the density of the unstable solutions when  $\sigma = 1$ , for  $s = 1$  and  $\delta = -1$ . The panels are initialized with (a weakly perturbed case example of) the antisymmetric solution for  $\mu = 0.19$  and  $0.25$  (left and right, respectively).

### Acknowledgments

PGK gratefully acknowledges support from the National Science Foundation under grants DMS-0806762 and CMMI-1000337, as well as by the Alexander von Humboldt Foundation through a Research Fellowship, the Alexander S. Onassis Public Benefit Foundation (grant RZG 003/2010-2011) and the Binational Science Foundation (grant 2010239). The work of PAT was partially supported by the State Scholarships Foundation in Greece. VMR gratefully acknowledges support from Research Council of AUTH (Grant 87872). This research has been co-financed by the European Union (European Social Fund - ESF) and Greek national funds through the Operational Program "Education and Lifelong Learning" of the National Strategic Reference Framework (NSRF) - Research Funding Program: THALES. Investing in knowledge society through the European Social Fund.

- 
- [1] C. Sulem and P. L. Sulem, *The Nonlinear Schrödinger Equation* (Springer-Verlag, New York, 1999).
  - [2] M.J. Ablowitz, B. Prinari and A.D. Trubatch, *Discrete and Continuous Nonlinear Schrödinger Systems*, Cambridge University Press (Cambridge, 2004).
  - [3] M. Albiez, R. Gati, J. Fölling, S. Hunsmann, M. Cristiani, and M. K. Oberthaler, Phys. Rev. Lett. **95**, 010402 (2005).
  - [4] T. Zibold, E. Nicklas, C. Gross and M.K. Oberthaler, Phys. Rev. Lett. **105**, 204101 (2010).
  - [5] S. Raghavan, A. Smerzi, S. Fantoni, and S. R. Shenoy, Phys. Rev. A **59**, 620 (1999); S. Raghavan, A. Smerzi, and V. M. Kenkre, Phys. Rev. A **60**, R1787 (1999); A. Smerzi and S. Raghavan, Phys. Rev. A **61**, 063601 (2000).
  - [6] E. A. Ostrovskaya, Yu. S. Kivshar, M. Lisak, B. Hall, F. Cattani, and D. Anderson, Phys. Rev. A **61**, 031601(R) (2000).
  - [7] K. W. Mahmud, J. N. Kutz, and W. P. Reinhardt, Phys. Rev. A **66**, 063607 (2002).
  - [8] V. S. Shchesnovich, B. A. Malomed, and R. A. Kraenkel, Physica D **188**, 213 (2004).
  - [9] D. Ananikian and T. Bergeman, Phys. Rev. A **73**, 013604 (2006).
  - [10] P. Ziń, E. Infeld, M. Matuszewski, G. Rowlands, and M. Trippenbach, Phys. Rev. A **73**, 022105 (2006).
  - [11] T. Kapitula and P. G. Kevrekidis, Nonlinearity **18**, 2491 (2005).
  - [12] G. Theocharis, P. G. Kevrekidis, D. J. Frantzeskakis, and P. Schmelcher, Phys. Rev. E **74**, 056608 (2006).
  - [13] D. R. Dounas-Frazer, A. M. Hermundstad, and L. D. Carr, Phys. Rev. Lett. **99**, 200402 (2007).
  - [14] T. Mayteevarunyoo, B. A. Malomed, and G. Dong, Phys. Rev. A **78**, 053601 (2008).
  - [15] C. Paré and M. Florjańczyk, Phys. Rev. A **41**, 6287 (1990); A. I. Maimistov, Kvant. Elektron. **18**, 758 (1991) [In Russian; English translation: Sov. J. Quantum Electron. **21**, 687; W. Snyder, D. J. Mitchell, L. Poladian, D. R. Rowland, and Y. Chen, J. Opt. Soc. Am. B **8**, 2102 (1991); P. L. Chu, B. A. Malomed, and G. D. Peng, J. Opt. Soc. Am. B **10**, 1379 (1993); N. Akhmediev, and A. Ankiewicz, Phys. Rev. Lett. **70**, 2395 (1993); B. A. Malomed, I. Skinner, P. L. Chu, and G. D. Peng, Phys. Rev. E **53**, 4084 (1996).
  - [16] C. Cambournac, T. Sylvestre, H. Maillotte, B. Vanderlinden, P. Kockaert, Ph. Emplit, and M. Haelterman, Phys. Rev. Lett. **89**, 083901 (2002).
  - [17] P. G. Kevrekidis, Z. Chen, B. A. Malomed, D. J. Frantzeskakis, and M. I. Weinstein, Phys. Lett. A **340**, 275 (2005).
  - [18] A. Griesmaier, J. Werner, S. Hensler, J. Stuhler, and T. Pfau, Phys. Rev. Lett. **94**, 160401 (2005); J. Stuhler, A. Griesmaier,

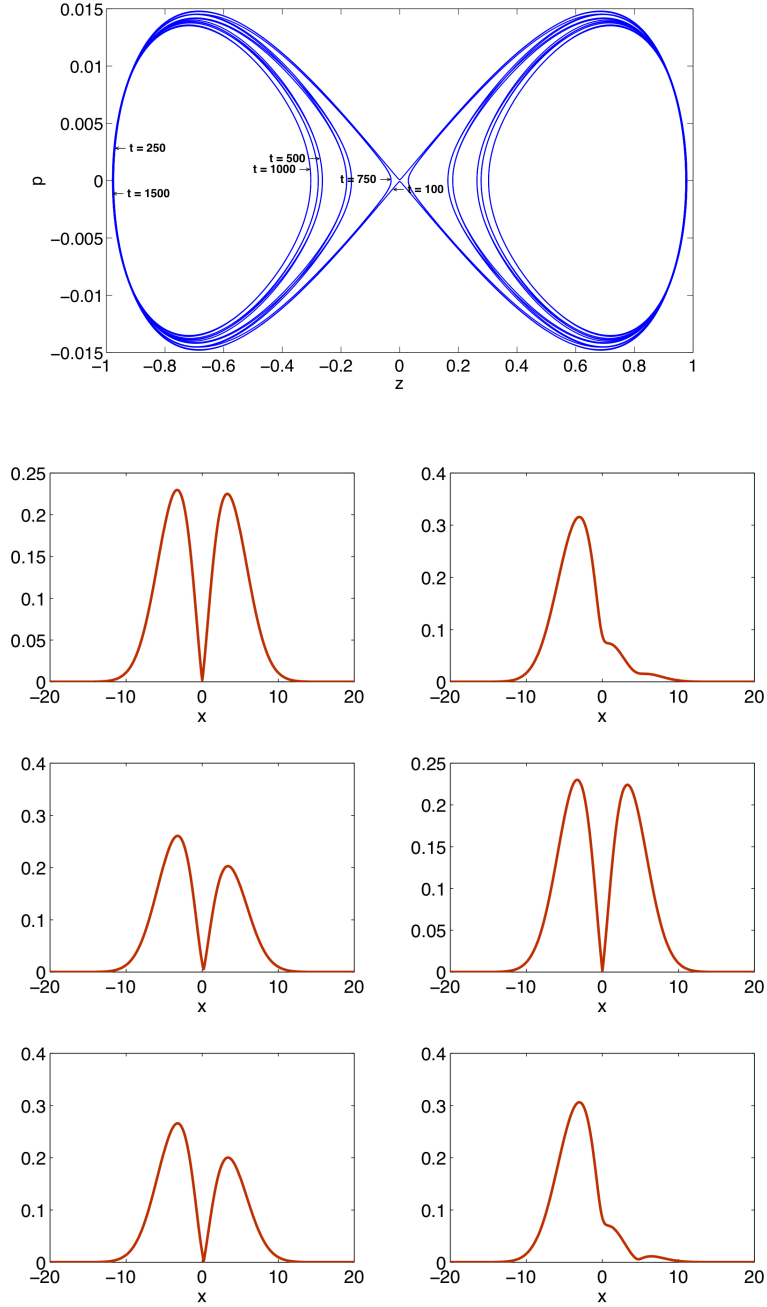


FIG. 11: Top panel: the numerically obtained trajectory of the solution for  $\mu = 0.19$ , for times between 0 and 1500. Rows below: the profiles of the solution for  $t = 100, 250$  (second row), 500, 750 (third row), 1000 and 1500 (fourth row).

- T. Koch, M. Fattori, T. Pfau, S. Giovanazzi, P. Pedri, and L. Santos, *ibid.* **95**, 150406 (2005); J. Werner, A. Griesmaier, S. Hensler, J. Stuhler, and T. Pfau, *ibid.* **94**, 183201 (2005); A. Griesmaier, J. Stuhler, T. Koch, M. Fattori, T. Pfau, and S. Giovanazzi, *ibid.* **97**, 250402 (2006); A. Griesmaier, J. Phys. B: At. Mol. Opt. Phys. **40**, R91 (2007); T. Lahaye, T. Koch, B. Fröhlich, M. Fattori, J. Metz, A. Griesmaier, S. Giovanazzi, and T. Pfau, Nature (London) **448**, 672 (2007).
- [19] T. Lahaye, C. Menotti, L. Santos, M. Lewenstein and T. Pfau, Rep. Progr. Phys. **72**, 126401 (2009).
- [20] B. Xiong, J. Gong, H. Pu, W. Bao, and B. Li, Phys. Rev. A **79**, 013626 (2009), M. Asad-uz-Zaman and D. Blume, *ibid.* **80**, 053622 (2009).

- [21] T. Köhler, K. Góral, and P. S. Julienne, *Rev. Mod. Phys.* **78**, 1311 (2006); J. Sage, S. Sainis, T. Bergeman, and D. DeMille, *Phys. Rev. Lett.* **94**, 203001 (2005); C. Ospelkaus, L. Humbert, P. Ernst, K. Sengstock, and K. Bongs, *ibid.* **97**, 120402 (2006); J. Deiglmayr, A. Grochola, M. Repp, K. Mörtlbauer, C. Glück, J. Lange, O. Dulieu, R. Wester, and M. Weidemüller, *ibid.* **101**, 133004 (2008); F. Lang, K. Winkler, C. Strauss, R. Grimm, and J. H. Denschlag, *ibid.* **101**, 133005 (2008).
- [22] M. Marinescu and L. You, *Phys. Rev. Lett.* **81**, 4596 (1998); S. Giovanazzi, D. O'Dell, and G. Kurizki, *Phys. Rev. Lett.* **88**, 130402 (2002); I. E. Mazets, D. H. J. O'Dell, G. Kurizki, N. Davidson, and W. P. Schleich, *J. Phys. B* **37**, S155 (2004); R. Löw, R. Gati, J. Stuhler and T. Pfau, *Europhys. Lett.* **71**, 214 (2005).
- [23] W. Królikowski, O. Bang, J. J. Rasmussen, and J. Wyller, *Phys. Rev. E* **64**, 016612 (2001); O. Bang, W. Królikowski, J. Wyller and J. J. Rasmussen, *Phys. Rev. E* **66**, 046619 (2002); J. Wyller, W. Królikowski, O. Bang and J. J. Rasmussen, *Phys. Rev. E* **66**, 066615 (2002).
- [24] D. Briedis, D. E. Petersen, D. Edmundson, W. Królikowski, and O. Bang, *Opt. Exp.* **13**, 435 (2005).
- [25] C. Rotschild, O. Cohen, O. Manela, and M. Segev, *Phys. Rev. Lett.* **95**, 213904 (2005).
- [26] A. Dreischuh, D.N. Neshev, D.E. Petersen, O. Bang, and W. Krolikowski *Phys. Rev. Lett.* **96**, 043901 (2006).
- [27] B. L. Lawrence and G. I. Stegeman. Two-dimensional bright spatial solitons stable over limited intensities and ring formation in polydiacetylene para-toluene sulfonate. *Optics letters*, **23**, 8 (1998) 591–593.
- [28] F. Smektala, C. Quemard, V. Couderc, and A. Barthélémy, *J. Non-Cryst. Solids* **274**, 232 (2000); G. Boudebs, S. Cheruklappurath, H. Leblond, J. Troles, F. Smektala, and F. Sanchez, *Opt. Commun.* **219**, 427 (2003).
- [29] C. Zhan et al., D. Zhang, D. Zhu, D. Wang, Y. Li, D. Li, Z. Lu, L. Zhao, and Y. Nie, *J. Opt. Soc. Am. B* **19**, 369 (2002).
- [30] G. S. Agarwal and S. Dutta Gupta, *Phys. Rev. A* **38**, 5678 (1988); E. L. Falcão-Filho, C. B. de Araújo, and J. J. Rodrigues, Jr, *J. Opt. Soc. Am. B* **24**, 2948 (2007).
- [31] R. A. Ganeev et al., M. Baba, M. Morita, A. I. Rysanyansky, M. Suzuki, M. Turu, H. Kuroda, *J. Opt. A: Pure Appl. Opt.* **6**, 282 (2004).
- [32] B. Gu, Y. Wang, W. Ji, and J. Wa, *Appl. Phys. Lett.* **95**, 041114 (2009).
- [33] K. Dolgaleva, H. Shin, and R. W. Boyd, *Phys. Rev. Lett.* **103**, 113902 (2009).
- [34] C. Wang, P.G. Kevrekidis, D.J. Frantzeskakis and B.A. Malomed, *Physica D* **240**, 805 (2011).
- [35] J. Yang, arXiv:1203.5148; and also arXiv:1204.2592.
- [36] P. Engels and C. Atherton *Phys. Rev. Lett.* **99**, 160405 (2007).
- [37] J. Marzuola and M.I. Weinstein, *Discr. Cont. Dyn. Sys. A* **28**, 1505 (2010).
- [38] T. Kapitula, P.G. Kevrekidis and Z. Chen, *SIAM J. Appl. Dyn. Sys.* **5**, 598 (2006).
- [39] R. Goodman, *J. Phys. A* **44**, 425101 (2011).
- [40] C. Wang, G. Theocharis, P.G. Kevrekidis, N. Whitaker, K.J.H. Law, D.J. Frantzeskakis and B.A. Malomed, *Phys. Rev. E* **80**, 046611 (2009).
- [41] It should be highlighted that this process is not uni-directional. More specifically, the harmonically trapped nature of the system may contribute to the reversal of the above described type of “flow”, leading to the eventual revisiting of outward trajectories.